PAPER

Check for updates

A biocompatible NIR squaraine dye and dye-antibody conjugates for versatile long-term *in vivo* fluorescence bioimaging†

Priyanka,[a] Galyna Bila,[bc] Sai Kiran Mavileti, [ID][a] Evgenia Bila,[d] Nazar Negrych,[b] Shekhar Gupta,[a] Linjun Tang,[a] Rostyslav Bilyy, [ID] *[bc] Shyam S. Pandey [ID] *[a] and Tamaki Kato*[a]

The demand for dependable near-infrared (NIR) probes, capable of sustained fluorescence within living systems and facile conjugation with biomolecules like antibodies and proteins, has been significantly on the rise, attributed to the substantial rise in the use of NIR imaging techniques and devices, with extensive integration into clinical diagnostics. Antibody conjugates are vital for targeted and selective bioimaging, enabling precise visualization of specific biomolecules within complex biological systems. Their multiplexing capability allows simultaneous detection of multiple targets, while their dynamic imaging capability enables real-time monitoring of cellular processes. Clinically, antibody conjugates have significant applications in disease prognosis, diagnosis, and monitoring. In this work, we report the synthesis of a new symmetrical NIR squaraine dye (**SQ-58**) with multiple carboxy anchoring groups for ease of coupling with antibodies. The dye showed decreased absorption and fluorescence intensity in phosphate buffer (PB) due to enhanced dye-aggregate formation. However, in the presence of bovine serum albumin (BSA) in PB, **SQ-58** showed an enhanced fluorescence signal along concentrations of BSA. **SQ-58** showed no cytotoxicity when tested in white laboratory mice while providing strong fluorescence when injected *in vivo*. Conjugation of **SQ-58** through the carboxylic groups to the isotypic mouse IgG antibodies (**IgG-SQ-58**) resulted in uniform distribution of the targeted molecule in the whole cardiovascular system. The NIR signal of **IgG-SQ-58** was stable for at least 7 days allowing the possibility of long-term imaging. Conjugation of **SQ-58** to antibodies raised against NK-Ly lymphoma tumor cells allowed efficient discrimination of tumor cells grown in the abdomen of laboratory mice. Thus, to the best of our knowledge, we report for the first time a biocompatible NIR dye, **SQ-58**, that can be easily conjugatable to biomolecules, and its antibody conjugates for a wide range of bioimaging applications.

1. Introduction

Bioimaging has revolutionized the field of biomedical research by providing a non-invasive means of observing specific biological activities with minimal disruption to the underlying processes. It plays a critical role in monitoring tissue and organ functions, as well as real-time changes in the biological environment for diagnostic and therapeutic purposes.[1,2] Among the various imaging techniques available, fluorescent probe-based bioimaging shows great promise due to its ability to enable real-time observations with exceptional sensitivity, high resolution, and non-invasiveness.[3,4]

Fluorescent probes offer valuable insights into the role of biomolecules and can be designed to target and study specific organelles in both healthy and diseased conditions.[5] Over the past decade, the development of highly effective fluorescence imaging probes, including quantum dots (QDs), rare-earth fluorescent crystals, organic dyes, fluorescent proteins/peptide-conjugates, nanomaterials, and carbon dots, has garnered significant interest. However, certain limitations such as high photobleaching rates, poor signal-to-noise ratio, short luminescence lifetimes, and

[a] *Graduate School of Life Science and System Engineering, Kyushu Institute of Technology, 2-4, Hibikino, Wakamatsu, Kitakyushu, 808-0196, Japan.*
E-mail: shyam@life.kyutech.ac.jp, tmkato@life.kyutech.ac.jp

[b] *Histology, Cytology & Embryology Department, Danylo Halytsky Lviv National Medical University, Pekarska Str. 69, 79010, Lviv, Ukraine.*
E-mail: r.bilyy@gmail.com

[c] *Lectinotest R&D, Mechanichna Str 2, 79000, Lviv, Ukraine*

[d] *Department of Organic Chemistry, Ivan Franko National University of Lviv, Kyrylo and Mefodiy Street 6, 79005, Lviv, Ukraine*

limited biocompatibility hinder the progress in developing fluorescent probes.[6–8]

To overcome these challenges, it is advantageous to utilize wavelength-tunable dyes that can absorb and emit light in the near-infrared (NIR) region of the electromagnetic spectrum. This is because absorption by tissue and blood, light scattering, and autofluorescence of biomolecules are less pronounced in the NIR range, leading to improved signal-to-noise ratio and deeper tissue penetration. The optical window of 650–900 nm and ∼1200–1450 nm is often considered ideal for *in vivo* imaging, as it minimizes interference from biological components.[9–11] Besides a growing list of affordable detectors working in the first region makes it of particular practical interest raising the demand for efficient fluorophores with emission of 650–900 nm. In recent years, there has been a growing global interest in the development of NIR fluorescent dyes and dye conjugates for bioimaging and biosensing applications.[12,13] These probes offer advantages such as minimal interference from biomolecules, reduced scattering, and enhanced tissue penetration.[14] However, challenges remain, as many commonly used fluorescent moieties, such as BODIPY,[15] rhodamine,[16] and coumarin,[17] have excitation wavelengths around 560 nm, limiting their suitability for deep tissue imaging and raising toxicity concerns. In this scenario, only a select few dye categories, such as phthalocyanine dyes,[18] cyanine dyes,[19] and squaraine dyes, exhibit suitability for NIR imaging.[20] However, some of these dyes are susceptible to oxidation in biological environments, resulting in the deterioration of their fluorescence and restricting the duration of observation following injection. Despite their NIR emission, the majority of other dye classes encounter issues such as photobleaching, *in vivo* instability, toxicity, limited versatility, and challenging synthetic pathways, in contrast to squaraine dyes making them more suitable for bioimaging applications.[21]

Squaraine (SQ) dyes are unique due to their unique electron-deficient central four-membered ring and a donor–acceptor–donor (D–A–D) configuration with electron-donating groups.[22] The distinct characteristics of SQ dyes, including their structural rigidity, tunable absorption wavelength, strong absorption properties, and excellent photothermal stability under ambient conditions, make them highly versatile for various applications.[23,24] Squaraine dyes have been used in various applications such as environmental sensing,[25] molecular sensing,[26,27] bioimaging,[20,28,29] and biochemical labeling.[30,31] However, the utilization of SQ dyes under physiological conditions faces constraints attributed to inherent chemical instability and self-aggregation in aqueous solutions. The fluorescence intensities of squaraine dyes are notably diminished as a consequence of aggregation, often resulting in complete quenching. Given that the development and exploration squaraine derivatives, hold tremendous potential for advancing bioimaging and biosensing techniques, it is important to address the limitations associated with existing dyes and optimizing their properties, thus paving way for improved imaging capabilities and deeper insights into biological systems.

On the other hand, protein target molecules, primarily of immune origin, such as low-affinity lectins[32] and high-affinity antibody conjugates are well established and have been used for targeted pathological cell visualization, drug delivery, photothermal therapy, *etc.*[33] On the other hand, conjugation of targeting proteins such as antibodies for imaging applications is quite a tedious process and can even lead to the loss of activity.[34,35] But on the bright side, antibody conjugates enable highly specific and targeted imaging of biological molecules or structures within complex systems such as cells, tissues, or organisms. By attaching fluorescent probes to antibodies that recognize specific antigens, visualization and tracking the localization of these targets with high precision can be achieved. The high affinity and specificity of antibodies ensure that imaging probes accumulate selectively at the target site, resulting in increased signal-to-noise ratios and improved detection sensitivity. Antibody conjugates allow for multiplexed imaging, where multiple targets can be simultaneously visualized within the same sample by conjugating antibodies with different fluorophores. Antibody conjugates also facilitate dynamic imaging studies by enabling real-time monitoring of cellular processes, protein–protein interactions, and signaling events. Antibody conjugates also have a significant clinical application in diagnostic imaging and disease monitoring. By targeting specific biomarkers associated with diseased states, antibody conjugates can be used for non-invasive imaging of tumors, inflammatory sites, and other pathological conditions, aiding in disease diagnosis, prognosis, and treatment monitoring.[36–40]

In this study, we report the synthesis and characterization of NIR symmetrical squaraine dye **SQ-58** anchoring multiple
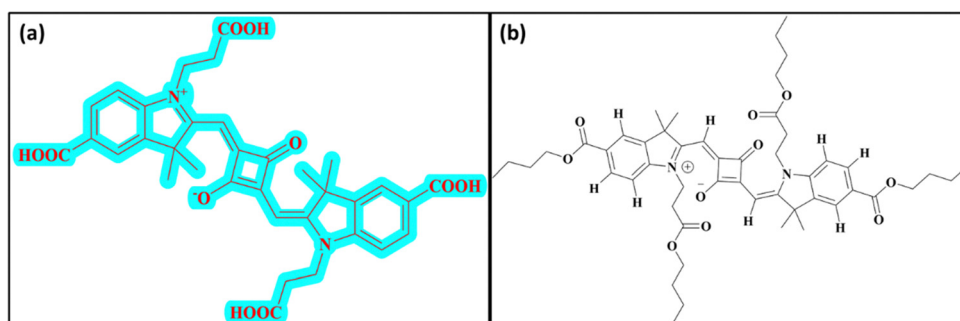

Fig. 1 Structure of dye used in this study: (a) **SQ-58** with multiple carboxy groups and (b) structure of **SQ-58**-butyl ester.

carboxy groups. The main advantage of multiple carboxy groups is to facilitate coupling with specific antibodies for targeted imaging of tissues and their microenvironment. Following the initial photophysical characterization in organic solvents and phosphate buffer, **SQ-58** was tested for its *in vivo* imaging capabilities. **SQ-58** when injected i.p. in white laboratory mice gave stable and strong fluorescence with no toxicity, and was excreted swiftly. Conjugation of **SQ-58** with isotypic mouse IgG antibodies resulted in uniform signal distribution in the whole cardiovascular system, and the NIR signal was stable for at least 7 days. Conjugation of **SQ-58** to antibodies raised against NK-Ly lymphoma tumor cells allowed efficient discrimination of tumor cells grown in the abdomen of laboratory mice, enabling long-term imaging.

2. Experimental

2.1. Material and methods

All the materials and general methods are elaborated in the ESI.†

2.2. Synthesis of SQ-58 and dye intermediates

SQ-58 (Fig. 1a) dye was synthesized as per Scheme 1. Detailed synthesis of **SQ-58** along with the corresponding intermediates are given in the ESI.†

2.3. Conjugation of SQ-58 with antibodies

SQ-58 was dissolved in DMSO at 10 mg per ml. IgG antibodies were dissolved at 1 mg ml^{-1} in 0.1 M MES buffer, pH 5, and dialyzed against this buffer. The following antibodies were used,
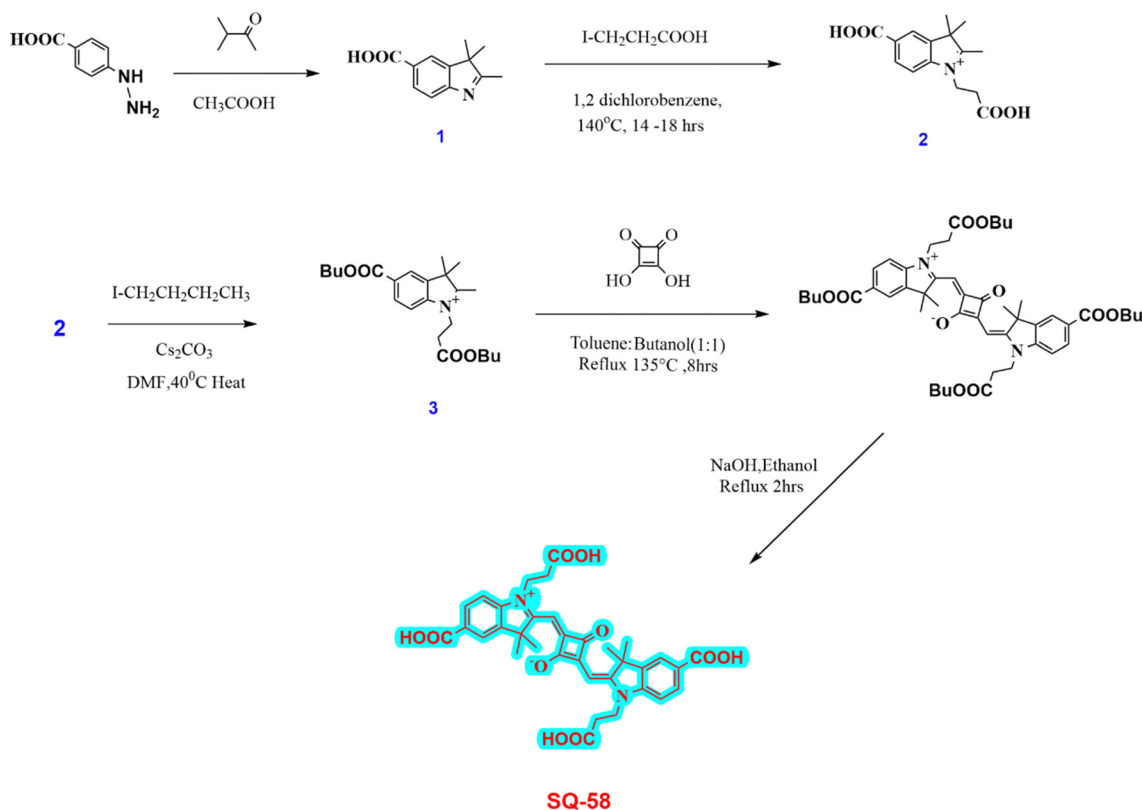
monoclonal mouse IgG1 isotype control of non-known specificity, MOPC (Xema, xema.fi) used to create unspecific **IgG-SQ-58**, and home-made rabbit polyclonal antibodies[41] against the membranous fraction of isolated lymphoma cells, purified by protein-G column was used to create the specific antitumor **aNK/Ly-IgG-SQ-58** conjugate to visualize NK/Ly-RB lymphoma cells.[42] **SQ-58** was mixed with the respective antibodies in MES buffer, 0.1 M, pH 5 (conjugation rate: 2 mg of protein/1 ml of **SQ-58**), followed by the addition of 1-ethyl-3-(3-dimethylaminopropyl) carbodiimide hydrochloride (EDC) [dry, MW 191.7, Sigma Aldrich] to obtain a 0.25 M solution. The reaction lasted 2 h at RT with constant stirring. The reaction mixture was purified by dialysis against 10 mM Tris buffer, pH 6.8. (If needed preserving compounds of choice can be added at this step).

2.3.1. Evaluation of conjugation efficiency by electrophoresis. Estimation of **SQ-58** conjugation efficiency and purification of the antibody conjugate was performed by agarose gel electrophoresis. 1% agarose gel in TEA buffer was used. 20 µL of **IgG-SQ-58** conjugate was loaded per well, along with **SQ-58** (diluted ten times in water) for reference, with bromophenol blue serving as the migration marker. Electrophoresis was performed at 50 V for one hour.[43] Since **SQ-58** provided a stained band, no additional staining was needed. Gel was photographed with a Nikon D7200 camera equipped with a macro lens.

2.4. Animal studies

White mice Balb/c were bred at the Animal House of Danylo Halytsky Lviv National Medical University (Lviv, Ukraine). The

Scheme 1 Synthesis of **SQ-58**.

animal studies were approved by the local ethical committee (Permission to R. Bilyy; 20200525/P4, 20180226/P2 and 2014-2018/P6) and conducted according to the guidelines of the Federation of European Laboratory Animal Science Associations (FELASA). Animals were kept in a clean environment, with water and food available *ad libitum*, under conditions of controlled temperature, humidity, and luminosity, under the professional supervision of veterinary doctors.

For tumor growth experiments mice weighing 30–35 g were used. For other experiments, 12-week-old mice weighing 20–25 g were used. Myeloid-type leukemia cells subcloned from Nemeth–Kellner - NK/Ly[42,44] were transplanted to Balb/c mice (1×10^6 NK/Ly-RB cells per mice) to induce liquid lymphoma-based tumor grown in ascites. After 7 to 10 days, when animal weight increased by 3 g and the ascites formation was visible, specific antitumor antibody conjugate **aNK/Ly-IgG-SQ-58** was injected *i.v.* under general anesthesia. To visualize blood and lymph vessels unspecific **IgG-SQ-58** (calculated to contain 20 μg of **SQ-58**) was injected i.p. under general anesthesia.[45]

2.5. *In vivo* imaging

In vivo imaging was performed using Li-COR Pearl Trilogy *In vivo* imager (LI-COR Biosciences GmbH, Germany). Excitation was performed with 685 and 785 nm lasers and emission was analyzed at 720 and 820 nm channels, respectively using a 85 μm resolution. Mice were subjected to general anesthesia and for kinetic measurement, the temperature of the detection chamber was maintained at 25 °C. Images were normalized using native Image Studio software, provided by the device manufacturer.

3. Results and discussion

3.1. Photophysical characterization

SQ-58 was successfully synthesized, purified, and then tested for photophysical properties using electronic absorption and fluorescence emission spectroscopy.

3.1.1 Solvatochromic study. Solvatochromism is the phenomenon of a molecule's color changing due to an alteration in the molecular environment created by the solvent molecules resulting in various interactions between the dye and solvent molecules.[46] Specifically, indole-based squaraines demonstrate strong photostability and fluorescence intensification in apolar media. Several substituted squaraines' solvent-dependent absorption and emission characteristics have been discovered, suggesting strong interactions in the ground and excited state. The photophysical behavior of **SQ-58** in different solvents was analyzed. The absorption maxima of **SQ-58** vary on the polarity of the solvent chosen. Table 1 summarizes the results of the photophysical parameters, while Fig. 2 shows **SQ-58**'s electronic absorption and fluorescence emission spectra in different solvents.

The solvatochromic behavior displayed by **SQ-58** in various solvent mediums can be explained by its interaction with the dipole moment of the solvent in both the ground and excited states post photoexcitation, along with hydrogen bonding interactions. Tang *et al.* previously reported such behavior in

Table 1 Photophysical characterization of SQ 58 in different solvents

Solvent	λ_{abs} (absorption maxima, nm)	λ_{emi} (Fluorescence emission maxima, nm)	Δ (Stokes shift, nm)
Methanol	650	670	20
Acetonitrile	646	665	19
Chloroform	658	675	17
DMF	663	680	17

squaraine dyes.[46] In the case of DMF, a well-known dipolar solvent with a high dielectric constant and a permanent dipole, serves as a poor hydrogen bond donor and acceptor. Consequently, there are minimal interactions with the dye's excited state, leading to fewer chances of forming H-aggregates responsible for inducing the blue shift, thus resulting in a redshifted λ_{max}. Conversely, methanol, being a protic solvent, acts as a relatively good hydrogen bond donor, increasing the likelihood of intermolecular interactions and the formation of H-aggregates leading to a blue shift. Observed in methanol, compared to chloroform, may be attributed to the non-polar nature of chloroform, where hydrogen bonding interactions are minimal, thus reducing the chances of forming H-aggregates.[46] The molar absorption coefficient (ε_o) in $CHCl_3$ was calculated to be 3.445×10^{-5} M^{-1} cm^{-1} by taking the absorption maxima corresponding to different concentrations of **SQ-58** (1 μM, 2 μM, 3 μM, 4 μM, and 5 μM) (Fig. S9, ESI†).

SQ-58 exhibited a Stokes shift ranging between 17 to 20 nm in the solvents used in this study. This relatively modest Stokes shift indicates the molecular rigidity, owing to minimal conformational changes occurring after photoexcitation.[47]

For quantum yield, rhodamine 6G whose Q_R is 0.95[48] was used as the reference, and the calculated fluorescence quantum (φ) yield of **SQ-58** was 0.16 in methanol, which is typical of squaraine dyes.[49,50]

3.1.2 Photophysical characterization in phosphate buffer and BSA interaction studies. Phosphate buffer solution (PB) has often been used to evaluate the interactions between dyes and biomolecules for sensing and imaging applications. In light of this, the electronic absorption and fluorescence emission spectra of 5 μM **SQ-58** in PB solution (pH 7.4) were measured, as shown in Fig. 3a and b.

SQ-58 showed decreased absorption and fluorescence intensity along with a blue shift in PB, owing to enhanced dye-aggregates formation. Owing to their flat molecular structure, squaraine dyes are well known to show dye aggregation. Squaraine dyes can form aggregates *via* non-covalent interactions, including π–π stacking, hydrophobic or hydrophilic interactions, van der Waals forces, electrostatic forces, and hydrogen bonding.[51,52] Typically, squaraine dyes exhibit two distinct types of aggregates: hypsochromically shifted H-aggregates, and bathochromically shifted J-aggregates[53] respective to the main monomeric peak. The absorption maxima of **SQ-58** in PBS is hypsochromically shifted to 640 nm (Fig. 3a) indicating the formation of H-aggregates leading to a decreased absorption and emission maxima (Fig. 3b). Understanding this aggregation-induced fluorescence quenching of squaraine dyes in aqueous
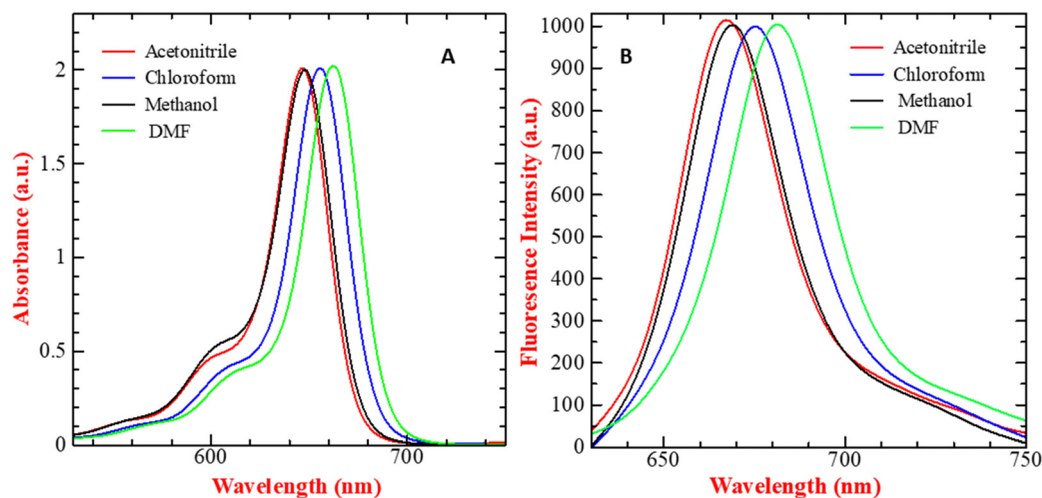
Fig. 2 (A) UV-Vis absorption spectra and (B) fluorescence emission spectrum (λ_{ex} = 610 nm, exitation and emission bandwidths are 5 and 6 respectivly) of 5 µM **SQ-58**-, in various solvents (normalized).

solutions is crucial for optimizing for applications such as biological imaging, as most of the bioimaging application needs to be carried out in aqueous media. In this context, model proteins like human serum albumin (HSA) and bovine serum albumin (BSA) have been employed to explore the interactions of probes with proteins for fluorescence enhancements. Given its substantial similarity in amino acid sequences to HSA, BSA has frequently served as a representative protein model for examining the interactions between dye and protein.[47,54,55] Hence, BSA interaction studies of **SQ-58** were conducted in PB.

As seen in Fig. 3c, two distinct sets of strong electronic absorption bands at 280 nm and 650–700 nm are observed corresponding to the absorption of BSA and **SQ-58**, respectively. With the increasing concentrations of BSA, the intensity of the band at 280 nm gradually increases, indicating that there is no denaturation of the BSA upon its interaction with the dye. The fluorescence emission spectrum of **SQ-58** in the presence of BSA is displayed in Fig. 3d. With increasing concentrations of BSA, the fluorescence intensity increased correspondingly accompanied by a redshift. This is attributed to the breaking of dye-aggregates owing to the dye–BSA interactions.[50]

To find out the extent of dye–BSA interactions and their relative association with BSA quantitatively, the apparent binding constant (K_a) was calculated according to the previously reported procedures.[47,56] As shown in Fig. 3e, the apparent binding constant (K_a) was calculated by plotting $(F_\infty - F_0)/(F_X - F_0)$ as a function of the inverse of BSA concentration. The value of K_a was calculated from the slopes of the figure, which was found to be 6.74×10^7 M, thus **SQ-58** displayed an extremely high binding affinity with BSA. This could be due to the presence of a hydrophilic carboxylic acid (COOH) functional group with a direct ring substitution that promotes hydrogen bonding with the binding sites of BSA.

3.2. SQ-58 conjugation to proteins

SQ-58 was conjugated with proteins employing the zero-length cross-linking method, using EDC as the coupling agent[57,58] (Fig. 4A). The unreacted product was effectively dialyzed and

the **IgG-SQ-58** conjugates were loaded on agarose gel (Fig. 4B) and separated. Migration of **SQ-58** alone, showed the forming of two bands, probably due to different charged forms, but in the case of **IgG-SQ-58** conjugates, the loaded product stayed in the well, as it was too big to be separated and no unconjugated dye was present. The ability to effectively eliminate unconjugated products is critical for *in vivo* imaging to prevent background fluorescence due to unconjugated dyes.

3.3. Toxicity of SQ-58 and its accumulation in the tissues of healthy animals

The goal of this experiment was to estimate the toxicity of **SQ-58** and to find the optimal dose for further *in vivo* experiments. Five mice were injected (i.p., injection volume: 100 µL) with 20 µg of **SQ-58** in 1% DMSO solution in 0.9% NaCl. The mice were weighed before the experiment (day 1) and on days 2, 4, and 7. No changes were detected in the animal behavior (monitored according to common practice[57]) on day 7 of the experiment, and all the mice appeared active and healthy. After the initial injection, the mice were subjected to anesthesia and were monitored for NIR fluorescence. One of the mice was sacrificed 4 h post-injection to study dye accumulation in organs. **SQ-58** was observed to be actively accumulating in the gastrointestinal system, especially in the liver and gallbladder of mice, and was then excreted into the intestine. Almost all fluorescent signal was observed in the colon, gallbladder, and some in the urinary bladder 4 h post-injection (Fig. 5). The fluorescence signal was highly decreased after 24 hours. On day 7, all mice were sacrificed and observed for internal organ damage, which was not observed. Furthermore, no statistically significant changes in the weight of the mice were observed upon their treatment with **SQ-58** during the observation time (Fig. S10, ESI†).

3.4. The use of SQ-58 antibody conjugates for tissue visualization

To test **SQ-58**'s ability for tissue labeling and imaging, the dye's stability in the body was first studied, as dyes tend to oxidize
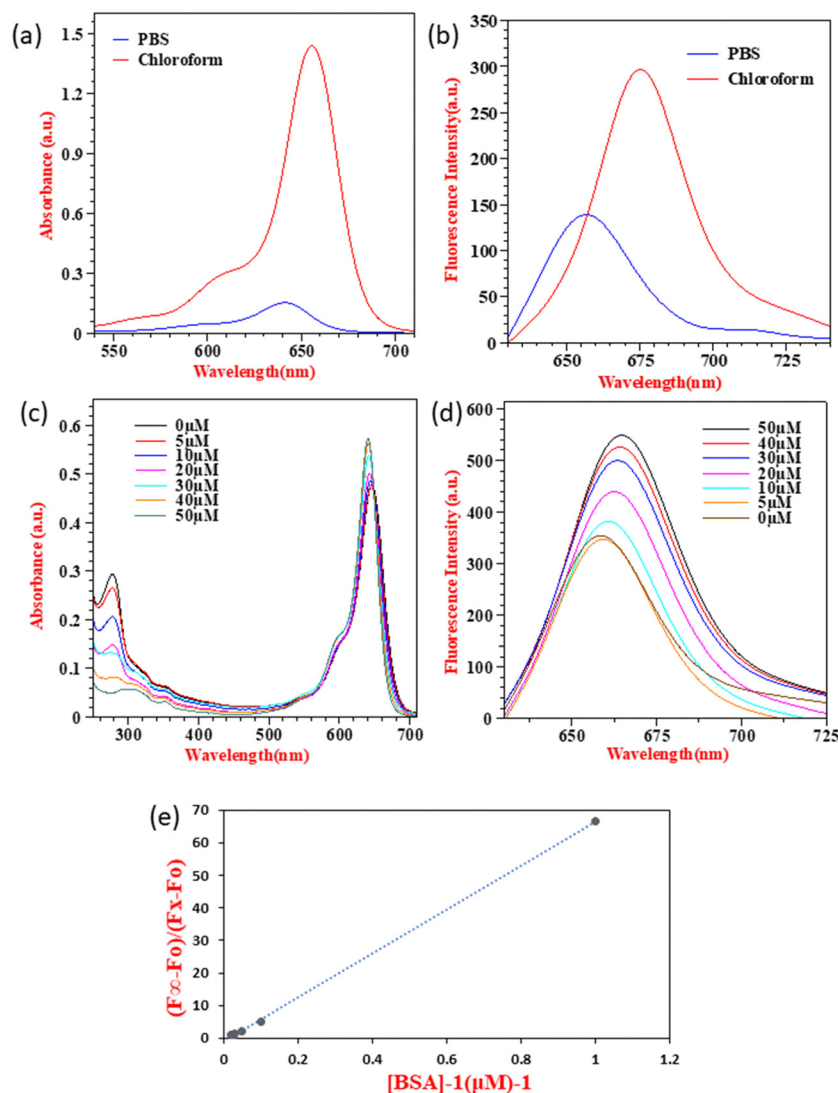
Fig. 3 Photophysical characterization in PB and BSA interaction studies of **SQ-58**: (a) electronic absorption spectra and (b) fluorescence emission spectrum of 5 μM **SQ-58** in PB and chloroform. (c) Electronic absorption spectra and (d) fluorescence emission spectra of 2 μM **SQ-58** in PB with varying concentrations of BSA (λ_{ex} = 610 nm, exitation and emission bandwidths are 5 and 6 respectivly). (e) The plot of $(F_\infty - F_0)/(F_X - F_0)$ vs. $[BSA]^{-1}$ at a fixed dye concentration of 2 μM.

and metabolize with time. To overcome this, **SQ-58** was conjugated to mouse monoclonal IgG with no defined specificity - MOPC (not binding any targets in the mouse body, but still perceived by the immune system of the mouse as self). In this case, the half-life of the IgG antibody molecule in the bloodstream (a few weeks) will be the defining parameter for the florescent compound to be detected. Injection of unspecific **IgG-SQ-58** conjugate i.p. resulted in almost immediate (1 min) distribution of conjugate in the mice vascular system showing uniform fluorescence (Fig. 6A), which then became concentrated in the intestinal system 4 h post-injection and was slowly released in feces (f, Fig. 6A). Uniform body staining was observed until 7 days when the experiment was terminated due to ethical requirements. Thus, **SQ-58** complexes with proteins are stable in bodies, not subjected to oxidation, and their half-life is defined only by the half-life of conjugated protein molecules.

Next, rabbit IgG targeting the plasma membrane of NK/Ly lymphoma tumors, produced in our laboratory, was used for conjugation with **SQ-58**. Mice were inoculated with tumor cells against which the antibody was raised and upon the tumor development, **aNK/Ly-IgG-SQ-58** conjugate was injected *i.v.* Since the tumor was developed in the intraperitoneal cavity and to ensure specificity, the injection of **aNK/Ly-IgG-SQ-58** was done *i.v.* Three hours post-injection, a dispersed fluorescence signal was evident within the abdominal region, encompassing the sites of tumor localization (Fig. 6B), thereby demonstrating the feasibility of achieving targeted imaging through the conjugation of **SQ-58** with specific recognition molecules.

4. Conclusion

In conclusion, a new symmetrical squaraine dye **SQ-58** with multiple carboxy groups, was successfully synthesized and
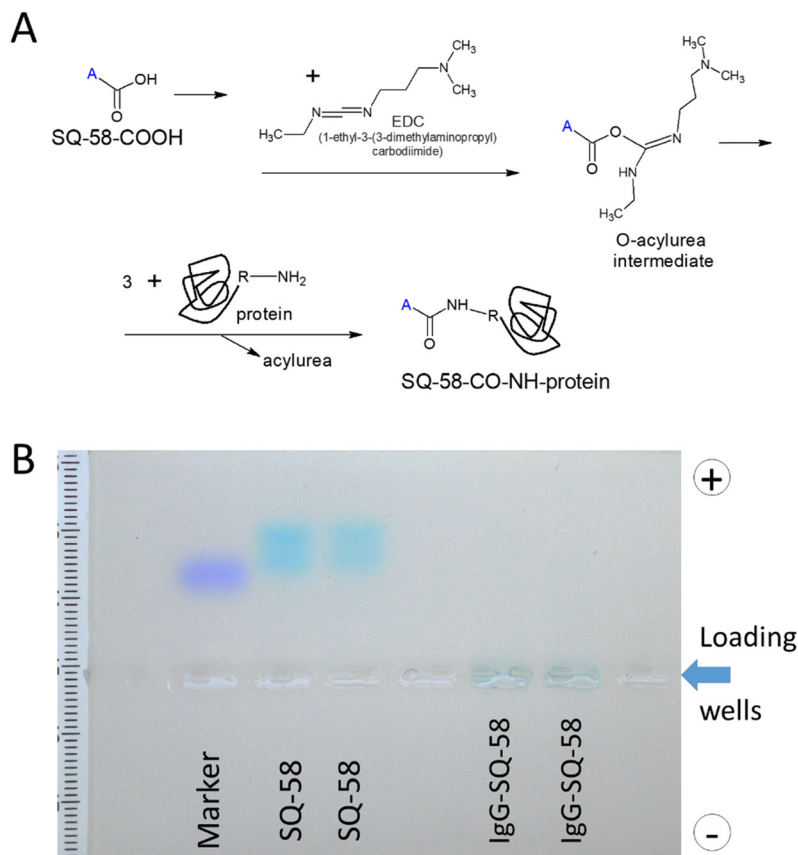
Fig. 4 (A) Schematic diagram of the conjugation of **SQ-58** to antibodies, and (B) Gel electrophoresis of **IgG-SQ-58**.
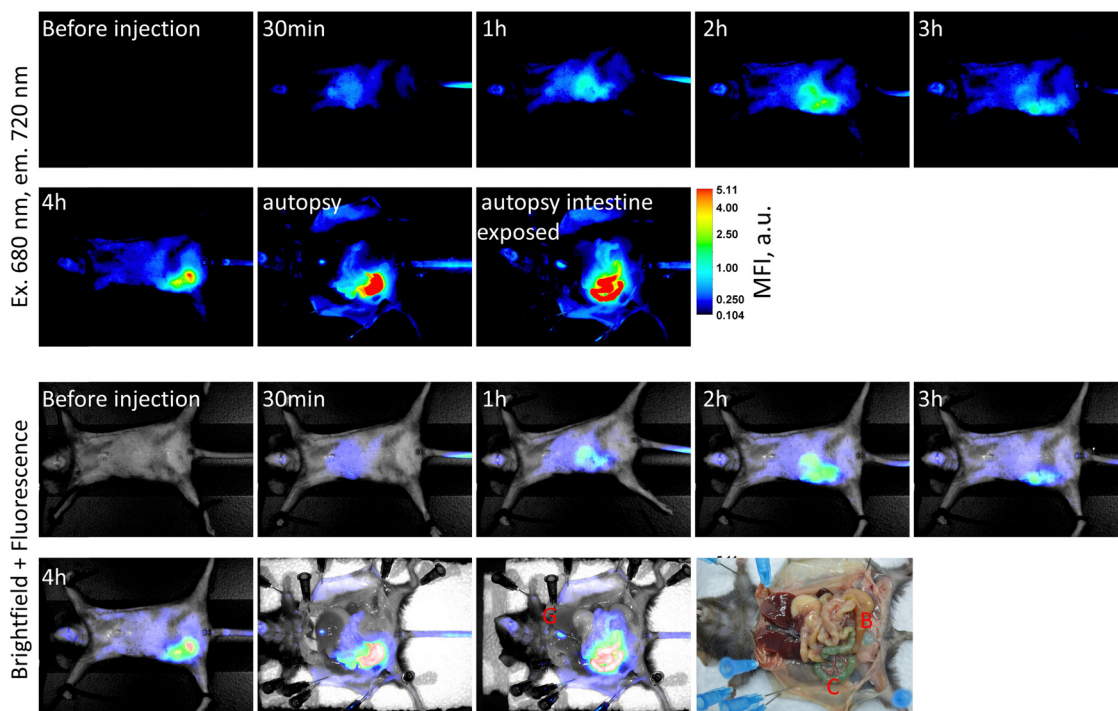

Fig. 5 Biodistribution of fluorescent signal in mice during first 4 hours post i.p. injection. Upper row: fluorescence readings. Lower row: brightfield images with fluorescence overlaid. The dye possesses a strong blue color observed in the colon insert. B – urinary bladder, C – colon, and G – gallbladder.
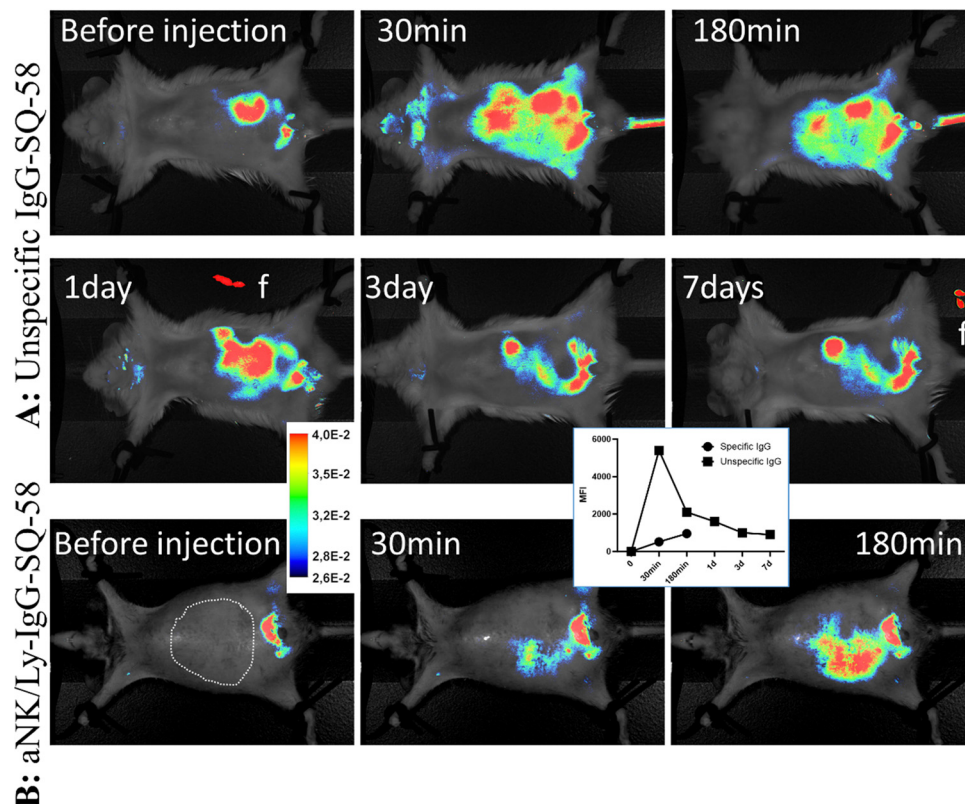
Fig. 6 Biodistribution of immunoglobulin molecules conjugated with **SQ-58**. (A) Un-specific **IgG-SQ-58** demonstrated uniform tissue distribution in the abdomen and was stable for up to 7 days, and feces (f-inset) demonstrated the way of compound excretion upon metabolism. (B) Specific anti-NK/Ly lymphoma IgG (**aNK/Ly-IgG-SQ-58**) allowed the detection of tumor masses (visualized by dotted areas). A typical out of 3 animals is presented. Inserts represent the pseudo coloring scale and mean MFI value during the course of measurements. The abdominal fur of mice was removed for better visualization.

characterized, demonstrating its absorption and emission properties in the NIR region. The dye's photophysical properties were evaluated in different solvents, revealing absorption at approximately 650 nm and emission at around 670 nm, with a Stokes shift of 20 nm. **SQ-58** showed decreased fluorescence intensity in phosphate buffer due to dye-aggregate formation. Interaction studies with BSA revealed the dye's potential for biosensing and bioimaging applications, as evidenced by enhanced fluorescence signals and a slight redshift of peak maxima upon increasing BSA concentration. *In vivo* studies demonstrated **SQ-58**'s biocompatibility and rapid excretion from the body *via* the bile and intestinal route. Conjugation of **SQ-58** with mouse IgG antibodies resulted in the uniform distribution of the targeted molecules within the cardiovascular system, with the created conjugate exhibiting stable NIR signals for at least seven days, enabling long-term imaging possibilities. Moreover, conjugating **SQ-58** with antibodies specific to NK-Ly lymphoma cells facilitated efficient discrimination of lymphoma tumor cells in laboratory mice. In summary, this study highlights the biocompatibility of the NIR dye **SQ-58**, and its un-specific **IgG-SQ-58** and specific **aNK/Ly-IgG-SQ-58** antibody conjugate, demonstrating its ease of conjugation with biological molecules, thus establishing it as a promising imaging candidate for a wide range of biomedical and clinical applications.

Author contributions

Conflicts of interest

The authors state that no personal, financial, or competing interests could otherwise have appeared to influence this reported review study.

Acknowledgements

References

1 H. S. Lahoti and S. D. Jogdand, *Cureus*, 2022, **14**, 1–8.

2 T. Yokoi, T. Otani and K. Ishii, *Sci. Rep.*, 2018, **8**, 4–6.

3 H. Zhu, J. Fan, J. Du and X. Peng, *Acc. Chem. Res.*, 2016, **49**, 2115–2126.

4 S. Lu, Z. Dai, Y. Cui and D.-M. Kong, *Biosensors*, 2023, **13**, 360.

5 H. Kobayashi, M. Ogawa, R. Alford, P. L. Choyke and Y. Urano, *Chem. Rev.*, 2010, **110**, 2620–2640.

6 F. Pinaud, X. Michalet, L. A. Bentolila, J. M. Tsay, S. Doose, J. J. Li, G. Iyer and S. Weiss, *Biomaterials*, 2006, **27**, 1679–1687.

7 K. M. Bratlie, T. T. Dang, S. Lyle, M. Nahrendorf, R. Weissleder, R. Langer and D. G. Anderson, *PLoS One*, 2010, **5**, 1–8.

8 R. Bilyy, A. Podhorodecki, M. Nyk, R. Stoika, A. Zaichenko, G. Zatryb, J. Misiewicz and W. Strek, *Phys. E*, 2008, **40**, 2096–2099.

9 S. Sreejith, K. P. Divya and A. Ajayaghosh, *Angew. Chem., Int. Ed.*, 2008, **47**, 7883–7887.

10 E. A. Owens, M. Henary, G. El Fakhri and H. S. Choi, *Acc. Chem. Res.*, 2016, **49**, 1731–1740.

11 V. J. Pansare, S. Hejazi, W. J. Faenza and R. K. Prud, *Chem. Mater.*, 2012, **24**, 812–827.

12 Y. Liu, J. M. Liu, D. Zhang, K. Ge, P. Wang, H. Liu, G. Fang and S. Wang, *J. Agric. Food Chem.*, 2017, **65**, 8229–8240.

13 J. Yu, X. Zhang, X. Hao, X. Zhang, M. Zhou, C. S. Lee and X. Chen, *Biomaterials*, 2014, **35**, 3356–3364.

14 S. Luo, E. Zhang, Y. Su, T. Cheng and C. Shi, *Biomaterials*, 2011, **32**, 7127–7138.

15 A. Loudet and K. Burgess, *Chem. Rev.*, 2007, **107**, 4891–4932.

16 J. Bucevičius, R. Gerasimaitė, K. A. Kiszka, S. Pradhan, G. Kostiuk, T. Koenen and G. Lukinavičius, *Nat. Commun.*, 2023, **14**, 1–14.

17 X. Y. Sun, T. Liu, J. Sun and X. J. Wang, *RSC Adv.*, 2020, **10**, 10826–10847.

18 G. M. Shivashimpi, S. S. Pandey, A. Hayat, N. Fujikawa, Y. Ogomi, Y. Yamaguchi and S. Hayase, *J. Photochem. Photobiol., A*, 2014, **289**, 53–59.

19 M. Saikiran, D. Sato, S. S. Pandey, T. Ohta, S. Hayase and T. Kato, *Dyes Pigm.*, 2017, **140**, 6–13.

20 J. O. Escobedo, O. Rusin, S. Lim and R. M. Strongin, *Curr. Opin. Chem. Biol.*, 2010, **14**, 64–70.

21 L. I. Markova, E. A. Terpetschnig and L. D. Patsenker, *Dyes Pigm.*, 2013, **99**, 561–570.

22 Y. Wang, Y. Li, Q. Yan, X. Liu, G. Xia, Q. Shao, K. Liang, L. Hong, B. Chi and H. Wang, *Dyes Pigm.*, 2020, **173**, 107977.

23 K. Ilina, W. M. MacCuaig, M. Laramie, J. N. Jeouty, L. R. McNally and M. Henary, *Bioconjugate Chem.*, 2020, **31**, 194–213.

24 B. Ostwald, F. Lehmann, L. Simon, E. Terpetschnig and O. S. Wolfbeis, *Anal. Biochem.*, 2000, **280**, 272–277.

25 J. J. McEwen and K. J. Wallace, *Chem. Commun.*, 2009, 6339.

26 J. V. Ros-Lis, B. García, D. Jiménez, R. Martínez-Máñez, F. Sancenón, J. Soto, F. Gonzalvo and M. C. Valldecabres, *J. Am. Chem. Soc.*, 2004, **126**, 4064–4065.

27 T. M. Kolev, D. Y. Yancheva and S. I. Stoyanov, *Adv. Funct. Mater.*, 2004, **14**, 799–805.

28 G. Patonay, J. Salon, J. Sowell and L. Strekowski, *Molecules*, 2004, **9**, 40–49.

29 B. Ostwald, L. Patsenker, J. Duschl, H. Szmacinski, O. S. Wolfbeis and E. Terpetschnig, *Bioconjugate Chem.*, 1999, **10**, 925–931.

30 J. R. Johnson, N. Fu, E. Arunkumar, W. M. Leevy, S. T. Gammon, D. Piwnica-Worms and B. D. Smith, *Angew. Chem.*, 2007, **119**, 5624–5627.

31 J. J. Gassensmith, E. Arunkumar, L. Barr, J. M. Baumes, K. M. DiVittorio, J. R. Johnson, B. C. Noll and B. D. Smith, *J. Am. Chem. Soc.*, 2007, **129**, 15054–15059.

32 R. O. Bilyy, V. O. Antonyuk and R. S. Stoika, *J. Mol. Histol.*, 2004, **35**, 829–838.

33 S. W. Fatima and S. K. Khare, *J. Controlled Release*, 2022, **341**, 555–565.

34 D. Li, R. S. Gamage, A. G. Oliver, N. L. Patel, S. Muhammad Usama, J. D. Kalen, M. J. Schnermann and B. D. Smith, *Angew. Chem.*, 2023, **62**, e202305062.

35 Y. Li, Y. Zhou, X. Yue and Z. Dai, *Adv. Healthcare Mater.*, 2020, **9**, 2001327.

36 D. Leung, J. Wurst, T. Liu, R. Martinez, A. Datta-Mannan and Y. Feng, *Antibodies*, 2020, **9**, 2.

37 M. Allam, S. Cai and A. F. Coskun, *npj Precis. Oncol.*, 2020, **4**, 11.

38 S. Kaur, G. Venktaraman, M. Jain, S. Senapati, P. K. Garg and S. K. Batra, *Cancer Lett.*, 2012, **315**, 97–111.

39 A.-H. Zarnani, M.-R. Nejadmoghaddam, M. M. Moghaddam, F. Mohammadi, M. Eskandari and R. Ghahremanzadeh, *Emerg. Mater. Res.*, 2018, **7**, 209–217.

40 S. L. Sahoo, C.-H. Liu, M. Kumari, W.-C. Wu and C.-C. Wang, *RSC Adv.*, 2019, **9**, 32791–32803.

41 A. Vaseruk, G. Bila and R. Bilyy, *Eur. J. Immunol.*, 2022, **52**, 123.

42 H. Gizem Özkan, V. Thakor, H. Xu, G. Bila, R. Bilyy, D. Bida, M. Böttcher, D. Mougiakakos, R. Tietze and A. Mokhir, *Chem. – Eur. J.*, 2022, **28**(30), e202104420.

43 T. Dumych, M. Lutsyk, M. Banski, A. Yashchenko, B. Sojka, R. Horbay, A. Lutsyk, R. Stoika, J. Misiewicz, A. Podhorodecki and R. Bilyy, *Croat. Med. J.*, 2014, **55**, 186–194.

44 S. Daum, M. S. V. S. V. Reshetnikov, M. Sisa, T. Dumych, M. D. M. D. Lootsik, R. Bilyy, E. Bila, C. Janko, C. Alexiou, M. Herrmann, L. Sellner and A. Mokhir, *Angew. Chem., Int. Ed.*, 2017, **56**, 15545–15549.

45 R. Bilyy, Q. Pagneux, N. François, G. Bila, R. Grytsko, Y. Lebedin, A. Barras, J. Dubuisson, S. Belouzard, K. Séron, R. Boukherroub and S. Szunerits, *Pathogens*, 2021, **10**, 861.

46 L. Tang, S. Sharma and S. S. Pandey, *Molecules*, 2022, **27**, 6578.

47 M. Saikiran, S. S. Pandey, S. Hayase and T. Kato, *J. Phys. Conf. Ser.*, 2017, **924**, 012006.

48 R. F. Kubin and A. N. Fletcher, *J. Lumin.*, 1982, **27** 455–462.

49 S. Gupta, Y. Yamawaki, S. Pradhan, S. S. Pandey and T. Kato, *Phys. Status Solidi*, 2023, **220**, 2300226.

50 S. K. Mavileti, G. Bila, V. Utka, E. Bila, T. Kato, R. Bilyy and S. S. Pandey, *ACS Appl. Bio Mater.*, 2024, **7**, 416–428.

51 M. Suzuki and K. Hanabusa, *Chem. Soc. Rev.*, 2010, **39**, 455–463.

52 S. De Feyter and F. C. De Schryver, *Chem. Soc. Rev.*, 2003, **32**, 139–150.

53 H. Chen, M. S. Farahat, K.-Y. Law and D. G. Whitten, *J. Am. Chem. Soc.*, 1996, **118**, 2584–2594.

54 M. Saikiran, D. Sato, S. S. Pandey, T. Ohta, S. Hayase and T. Kato, *Dyes Pigm.*, 2017, **140**, 6–13.

55 M. B. E. Turbay, V. Rey, N. M. Argañaraz, F. E. Morán Vieyra, A. Aspée, E. A. Lissi and C. D. Borsarelli, *J. Photochem. Photobiol., B*, 2014, **141**, 275–282.

56 L. Tarazi, N. Narayanan and G. Patonay, *Microchem. J.*, 2000, **64**, 247–256.

57 R. Bilyy, A. Tomyn, Y. Kit, A. Podhorodecki, J. Misiewicz, M. Nyk, W. Strek and R. Stoika, *Materialwissenschaft und Werkstofftechnik*, 2009, vol. 40, pp. 234–237.

58 G. T. Hermanson, *Bioconjugate Techniques*, Academic Press, London, 3rd edn, 2013.